A Journal of the Gesellschaft Deutscher Chemiker
Angewandte
GDCh
International Edition
Chemie
www.angewandte.org

Accepted Article

Title: A Dual Threat: Redox-Activity and Electronic Structures of Well-Defined Donor-Acceptor Fulleretic Covalent-Organic Materials

Authors: Natalia B. Shustova, Gabrielle A. Leith, Allison M. Rice, Brandon J. Yarbrough, Anna A. Berseneva, Richard T. Ly, Charles N. Buck, Amy J. Brandt, Donna A. Chen, Benjamin W. Lamm, Morgan Stefik, Kenneth S. Stephenson, Mark D. Smith, Aaron K. Vannucci, Perry J. Pellechia, Sophya Garashchuk, and Denis Chusov

To be cited as: *Angew. Chem. Int. Ed.* 10.1002/anie.201914233
Angew. Chem. 10.1002/ange.201914233

Link to VoR: http://dx.doi.org/10.1002/anie.201914233
http://dx.doi.org/10.1002/ange.201914233

WILEY-VCH

10.1002/anie.201914233

WILEY-VCH

COMMUNICATION

A Dual Threat: Redox-Activity and Electronic Structures of Well-Defined Donor-Acceptor Fulleretic Covalent-Organic Materials

Gabrielle A. Leith,[a]§ Allison M. Rice,[a]§ Brandon J. Yarbrough,[a]§ Anna A. Berseneva, [a] Richard T. Ly,[a] Charles N. Buck III,[a] Denis Chusov,[b] Amy J. Brandt,[a] Donna A. Chen,[a] Benjamin W. Lamm, [a] Morgan Stefik,[a] Kenneth S. Stephenson,[c] Mark D. Smith,[a] Aaron K. Vannucci,[a] Perry J. Pellechia,[a] Sophya Garashchuk,[a] and Natalia B. Shustova*[a]

Abstract: The effect of donor (D)-acceptor (A) alignment on the materials electronic structure was probed for the first time using novel purely organic porous crystalline materials with covalently integrated two- and three-dimensional acceptors. The first studies towards estimation of charge transfer rates as a function of acceptor stacking are in line with the experimentally observed, drastic (*ca* eight-fold) conductivity enhancement. Redox behavior of prepared materials, which are the first studies of this kind reported for any buckyball- or tetracyanoquinodimethane-integrated crystalline porous scaffolds to date, was evaluated. Moreover, in parallel with tailoring the D-A alignment responsible for "static" changes in materials properties, an external stimulus was applied for the first time to this class of materials for "dynamic" control of the materials' electronic profiles. Overall, the discussed D-A strategic design, in combination with stimuli-controlled electronic behavior, redox activity, and modularity could be used as a blueprint for the development of electroactive and conductive multidimensional and multifunctional crystalline porous materials.

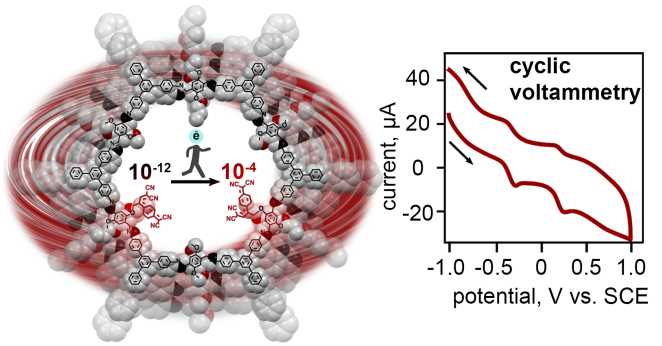

Scheme1. (*left*) Donor-acceptor alignment inside of a porous well-defined organic framework resulting in conductivity enhancement. (*right*) The cyclic voltammetry curve of crystalline porous material with embedded electron-accepting moieties (TCNQ[**1≡(34%)**]; DMF solution containing 0.1 M tetrabutylammonium hexafluorophosphate, TCNQ[**1≡(34%)**] (40 wt.%), carbon black (60 wt.%), and 0.1 mL of Nafion; saturated calomel reference, platinum wire counter, and gold working electrodes).

Merging the properties of three-dimensional buckyballs (or buckybowls) and covalent-organic frameworks (COFs) provides access to a novel class of materials combining ultrafast energy/electron transport characteristic of three-dimensional (3D) fulleretic linkers with high modularity, crystallinity, and surface area, which are intrinsic properties of COFs.[1-13] The precise donor-acceptor alignment achieved in the materials is imposed by the rigid COF scaffold and is crucial for efficient energy or charge transfer as it can influence the distance of exciton diffusion, π-π stacking, or Förster radius, and as a result, can enhance device performance.[14–20]

Herein, we demonstrate that the donor-acceptor alignment in well-defined frameworks could drastically affect the materials' electronic properties resulting in *ca* 100,000,000-fold conductivity enhancement, one of the largest increases reported for COFs.[21–30] We probed charge transfer rates within the Marcus theory as a function of acceptor stacking. In addition, we estimated redox behavior using cyclic voltammetry of *pure organic* crystalline porous scaffolds containing covalently decorated pores with strong electron accepting bound tetracyanoquinodimethane (TCNQ) and fullerene (C_{60}) moieties,[31–33], which are the first studies of this kind reported for any buckyball- or TCNQ-integrated COFs to date. We demonstrate that the concept of fluorophore tag integration could be an effective avenue to monitor reaction progress inside of a COF. To achieve that, the COF interior for the first time was harnessed for performance of Sonogashira cross-coupling and [2+2] cycloaddition reactions, followed by ring opening of a strained cyclobutene intermediate in the case of the latter. In addition to donor (COF)-acceptor (fullerene or TCNQ) alignment responsible for "static" changes in the materials' electronic structure, we also test the hypothesis that an excitation wavelength could be used for dynamic control of electronic properties in COFs infiltrated with photoresponsive units as a function of an external stimulus for the first time.[34–36]

For integration of three-dimensional (3D) acceptors such as buckyballs, choice of the host matrix (COF) should satisfy the following criteria: (i) sufficient pore aperture for accommodation of bulky electron acceptors (e.g., C_{60} diameter ~7 Å;), (ii) presence of reactive functional groups promoting cycloaddition or coupling reactions, and (iii) maintenance of structural integrity after derivatization. The first two strategies (1,3- and [2+2] cycloaddition followed by ring opening of a strained intermediate) were utilized to integrate 3D and planar electron acceptors while the third strategy (Sonogashira cross-coupling) was employed to embed fluorophore tags (vide infra). The COF, **1≡(x%)** (where x = 34 = [BPTA]/([BPTA]+[DMTA]) × 100%; Figure 1), prepared from 2,5-bis(2-propynyloxy)

[a] G. A. Leith,§ A. M. Rice, § B. J. Yarbrough, § A. A. Berseneva, R. T. Ly, C. N. Buck III, A. J. Brandt, Prof. Dr. D. A. Chen, B. W. Lamm, Prof. Dr. M. Stefik, Dr. M. D. Smith, Prof. Dr. A. K. Vannucci, Dr. P. J. Pellechia, Prof. Dr. S. Garashchuk, and Prof. Dr. N. B. Shustova
§ equal contribution
Department of Chemistry and Biochemistry, University of South Carolina (USC)
631 Sumter Street, Columbia, SC 29208 (USA)
E-mail: shustova@sc.edu
[b] Dr. D. Chusov
A. N. Nesmeyanov Institute of Organoelement Compounds of the Russian Academy of Sciences
Vavilova St. 28, Moscow 119991, Russian Federation
[c] K. S. Stephenson
Department of Physics and Astronomy, USC
712 Main Street, Columbia, SC 29208 (USA)
Supporting information for this article is given via a link at the end of the document.

10.1002/anie.201914233

terephthalaldehyde (BPTA), 2,5-dimethoxyterephthalaldehyde (DMTA), and tri-(4-aminophenyl)benzene (TAPB), satisfies the mentioned criteria. This COF (i) possesses 30 Å-channels, (ii) contains alkyne groups available for postsynthetic derivatization (see the Supporting Information for synthetic details), and (iii) maintains structural integrity over a wide pH range.[37]

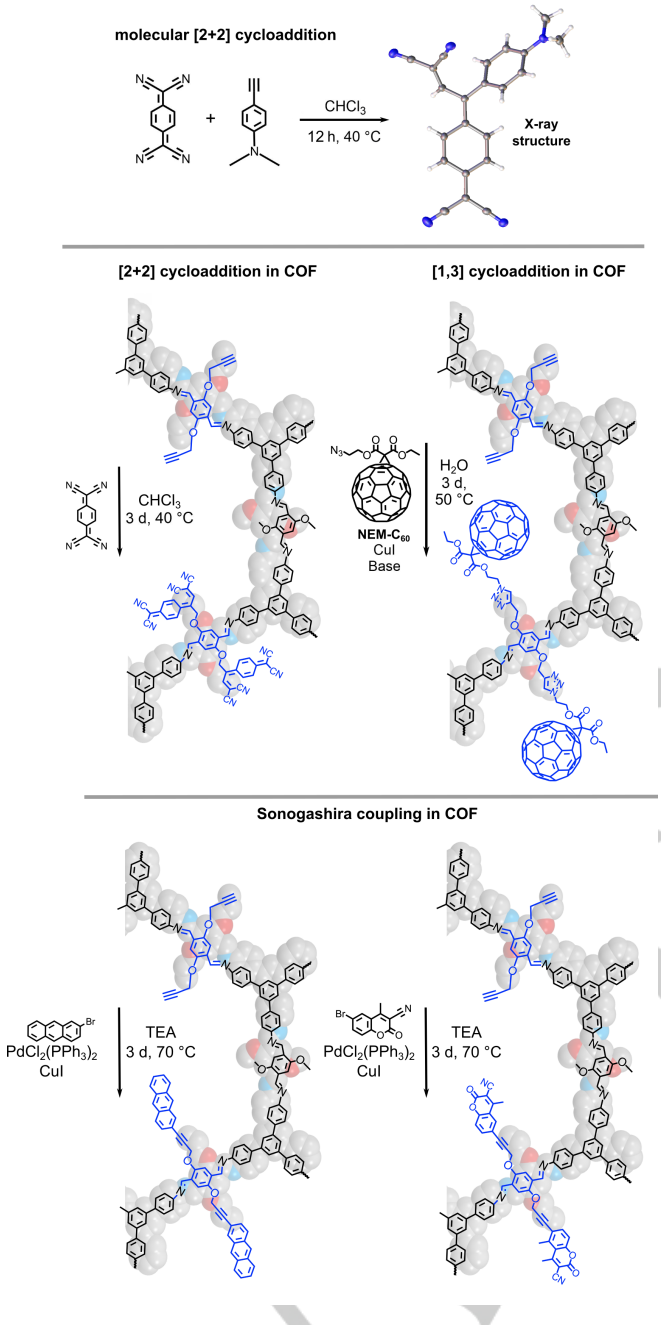

Figure 1. (*top*) Development of reaction conditions utilizing molecular TCNQ moieties for the [2+2] cycloaddition reaction, followed by ring opening of a strained cyclobutene intermediate. Single-crystal X-ray structure of the product is shown. Thermal displacement ellipsoids are drawn at the 50% probability level. (*middle*) The 1,3-cycloaddition and [2+2] cycloaddition reactions, followed by ring opening of a strained cyclobutene intermediate in the case of the latter, for integration of fullerene and TCNQ moieties, respectively, are shown. (*bottom*) Integration of a fluorescent tag using Sonogashira cross-coupling reaction.

Prior to investigations with bulky and relatively expensive fullerene-containing derivatives, we systematically studied the reaction conditions suitable for 1,3-cycloaddition starting with less bulky and more affordable azide-based derivatives, e.g., 2-azidoethanol and 2-azidoethyl ethyl malonate.Only after such control experiments, where the reaction conditions which were developed for cycloaddition of the small azide-based derivatives, applied for integration of 2-azidoethyl ethyl malonate (NEM) inside the of the COF (**1≡(34%)**, see the Supporting Information). As a result, the methodology for development of donor-acceptor materials includes two-steps: (i) several-day pre-soaking of, for instance, C_{60} derivatives inside the large COF channels promoting acceptor diffusion and (ii) addition of the reagents required for a 1,3-cycloaddition reaction (Figure 1) followed by heating. Synthesis of the C_{60} derivative, 2-azidoethyl-(ethyl)-3'*H*-cyclopropa-[1,2](C60)[5,6]fullerene-3',3'-dicarboxylate (NEM-C_{60}, Figure 1), suitable for the cycloaddition reaction and accessible on a gram-scale without the use of labor-demanding high-pressure liquid chromatography (HPLC) was performed using a 3-step procedure.[38]

Spectroscopic techniques including Fourier-transform infrared (FTIR) and solid-state ^{13}C cross-polarization magic-angle spinning (CP-MAS) nuclear magnetic resonance (NMR) spectroscopies, as well as fluorophore tag integration discussed below, were used to monitor reaction progress in the solid state. Control experiments, in which the COF was subjected to the same reaction conditions but without the addition of the azide-containing precursor, were also carried out. In the case of FTIR spectroscopic studies, we monitored the disappearance of 2120 cm^{-1} (C≡C) and 3300 cm^{-1} (C≡C–H) bands (Figures 2 and 3) in the spectra of products in contrast to the control experiment where both bands were preserved (Figure S11). For instance, in the case of NEM-C_{60}[**1≡(34%)**], FTIR spectroscopic studies confirmed disappearance of the C≡C resonance as well as appearance of the carbonyl stretch (1716 cm^{-1}) of the diethyl malonate moiety (Figure 2). The ^{13}C CP-MAS spectroscopic studies of NEM-C_{60}[**1≡(34%)**] demonstrated disappearance of the C≡C resonances in contrast to the control experiment (without presence of the azide precursor under the same reaction conditions, Figure 2). Moreover, the substantial decrease of Brunauer-Emmett-Teller (BET) surface area from 1253 m^2g^{-1} (**1≡(34%)**, Figure S15) to 229 m^2g^{-1} (NEM-C_{60}[**1≡(34%)**], Figure S16) also supports incorporation of bulky C_{60} derivatives inside of the porous scaffold. Although the surface area for a covalently linked C_{60}-metalloporphyrin COF was slightly higher (393 m^2/g),[39] we report the highest surface area determined for a purely organic COF with covalently bound C_{60} acceptors to date. The steady-state and time-resolved spectroscopic studies are also in line with integration of electro accepting units inside of the electron donating host (vide infra). Crystallinity of the synthesized material was preserved even after multiple cycles of the 1,3-cycloaddition reaction necessary for maximization of C_{60} content as evident through wide-angle X-ray scattering (WAXS, Figure S9) studies; resulting in the first example of a crystalline, porous, and fully organic covalently-linked C_{60}-based COF. [39–42]

While C_{60} possesses a unique spherical structure allowing for stabilization of up to six electrons, the LUMO of C_{60} (–4.50 eV) is comparable with a planar acceptor, TCNQ (–4.23 eV).[43,44] TCNQ derivatives usually do not require the labor-intensive HPLC procedure for their isolation, in contrast to C_{60} compounds with a large number of active centers and possible isomers,[14] making it possible to compare the properties of prepared NEM-C_{60}[**1≡(34%)**] with TCNQ-covalently-linked analogs. To develop suitable reaction conditions to perform a [2+2] cycloaddition

10.1002/anie.201914233

reaction followed by ring opening of an intermediate cyclobutene necessary to attach TCNQ through a covalent bond to the COF interior and to monitor reaction progress using “conventional”

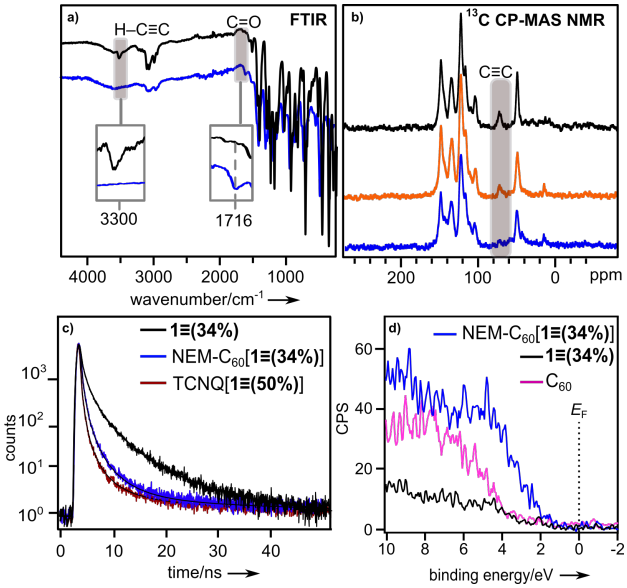

Figure 2. (a) FTIR spectra of **1≡(34%)** (black) and NEM-C_{60}[**1≡(34%)**] (blue). Grey areas show H–C≡C present in **1≡(34%)** and absent in NEM-C_{60}[**1≡ (34%)**] and the appearance of the C=O stretch in NEM-C_{60}[**1≡ (34%)**]. (b) ^{13}C CP-MAS NMR spectra of **1≡(34%)** (black), a control experiment with **1≡(34%)** (orange), and NEM-C_{60}[**1≡(34%)**] (blue). (c) Fluorescent decays of **1≡(34%)** (black), NEM-C_{60}[**1≡(34%)**] (blue), and TCNQ[**1≡ (50%)**] (red). (d) XPS data for the valence band region for **1≡(34%)** (black), C_{60} (pink), and NEM-C_{60}[**1≡ (34%)**] (blue).

solution NMR spectroscopy, we started with the molecular building blocks, TCNQ and 4-ethynyl-*N,N*-dimethylaniline (Figure 1). In addition to spectroscopic studies, formation of the desired product, 2-(4-(4,4-dicyano-2-(4-(dimethylamino)phenyl)butylidene)cyclohexa-2,5-dien-1-ylidene)malononitrile, was confirmed by single-crystal X-ray crystallography (Figures 1 and S12). As a next step, the developed conditions were applied toward the reaction of TCNQ with the COF (**1≡(x%)**). For comprehensive characterization of the prepared TCNQ[**1≡(x%)**], we used the same set of techniques as in the case of NEM-C_{60}[**1≡(34%)**]. For instance, we observed disappearance of 2120 cm^{-1} (C≡C) and 3300 cm^{-1} (C≡C–H) bands in the FTIR spectrum, while appearance of the nitrile stretch at 2100 cm^{-1} (C≡N) persisted even after a 24-hour Soxhlet washing procedure, highlighting the presence of TCNQ covalently bound to the COF (Figure 3). Due to the smaller size of TCNQ versus the relatively bulky NEM-C_{60}, the measured BET surface area even after TCNQ integration was found to be 812 m^{2}g^{-1} (Figure S17). The determined surface area is the highest for a TCNQ-covalently-linked COF to date in comparison with previous reports that mainly focused on infiltration of TCNQ molecules as guests.[23]

In addition to spectroscopic methods and gas sorption analysis, fluorescent labeling was utilized to address the question about residual unreacted alkyne sites. Two chromophores, 6-bromo-3-cyano-4-methylcoumarin and 2-bromoanthracene, were selected to perform a Sonogashira cross-coupling reaction within the functionalized COF (Figure 1). As a control experiment, we integrated coumarin and anthracene moieties inside **1≡(50%)**. We observed a strong fluorescent signal for both anthracene[**1≡(50%)**] and 4-methyl-2-oxo-2*H*-chromene-3-carbonitrile[**1≡(50%)**] (Figures S22 and S23). We applied the developed strategy towards detection of residual alkyne moieties in TCNQ[**1≡(50%)**]. In contrast to the reaction with **1≡(50%)**, there was no emission detected for TCNQ[**1≡(50%)**] after the treatment with both fluorescent tags (Figures S24–25). These findings are in line with the spectroscopic evidence and confirm the lack of unreacted alkyne sites concluding reaction completion.

To study the electronic and photophysical properties of the prepared donor-acceptor materials, comprehensive analysis including diffuse reflectance (DR), steady-state and time-resolved photoluminescence (PL), and X-ray photoelectron (XPS) spectroscopies, cyclic voltammetry (CV), and conductivity measurements were employed.

Integration of electron acceptors (TCNQ or C_{60}-derivative) inside the COF was accompanied by a drastic color change from pale yellow to dark red or brown, respectively (Figure 3). DR spectroscopic studies confirm that acceptor integration resulted in the appearance of an additional absorption band leading to a bathochromic shift of the absorption profile in comparison with the parent COF, C_{60}, and TCNQ, which is typically associated with charge transfer (CT).[31,45] To further study the observed behavior of both C_{60} and TCNQ-modified COFs, we utilized time-resolved PL spectroscopy. With the assumption that the PL decay rate consists of radiative, nonradiative, and CT components, analysis should reveal shortening of PL lifetimes of the host owing to integration of strong acceptor moieties (i.e., fullerene-based derivative or TCNQ).[46] The amplitude-averaged lifetime estimated by fitting the time-resolved PL decay curves were 474 ps for **1≡(34%)** while NEM-C_{60}[**1≡(34%)**] and TCNQ[**1≡(50%)**] exhibited much shorter lifetimes of 32 ps and 103 ps, respectively. This is indicative of the potential for CT in the system (Figure 2). Similar behavior was previously reported in literature for C_{60} inclusion as guest molecules.[41] In addition, the emission response of the COF itself was quenched when either TCNQ or NEM-C_{60} was covalently bound to the COF walls (Figure S27).

As a fast and nondestructive pre-screening technique, XPS was used to probe the electronic structure of the C_{60}-based COF by monitoring the density of states (DOS) near the Fermi level (E_F, binding energy = 0 eV). For **1≡(34%)** itself, the valence band spectrum exhibits behavior associated with insulating materials, given that there is near zero intensity within 3 eV of the Fermi level (E_F = 0 eV binding energy). The spectrum of C_{60} also shows zero intensity at 3 eV. In contrast, the XPS valence band spectrum for NEM-C_{60}[**1≡(34%)**] exhibits higher intensity at 3 eV from E_F. This indicates a greater DOS near E_F, which would be consistent with a more conductive material.

To further elaborate on the observed changes in the XPS spectra, we performed conductivity measurements demonstrating that, for instance, the conductivity of NEM-C_{60}[**1≡(34%)**] was found to be 1.97 × 10^{-6} S/cm in comparison with the parent COF (2.32 × 10^{-12} S/cm).[31] Our observations that conductivity increases with promotion of donor-acceptor alignments are in line with literature reports.[32] On the example of TCNQ-integrated materials, we also studied changes in electronic properties as a function of the degree of acceptor integration. Conductivity measurements demonstrate an order-of-magnitude difference for TCNQ[**1≡(34%)**] (1.67 × 10^{-7} S/cm) versus TCNQ[**1≡(100%)**] (2.12 × 10^{-6} S/cm) resulting in a six-orders-of-magnitude increase in comparison to the COF itself (2.32 × 10^{-12} S/cm). The optical band gap values derived from the Tauc plot analysis for **1≡(34%)**, NEM-C_{60}[**1≡(34%)**], and TCNQ[**1≡(50%)**] were found to be 2.32

10.1002/anie.201914233

eV, 1.81 eV, and 2.04 eV, respectively, and they are in line with the conductivity measurements (Figures S34-35).[47,48] Further tuning of electronic properties was achieved through iodine doping

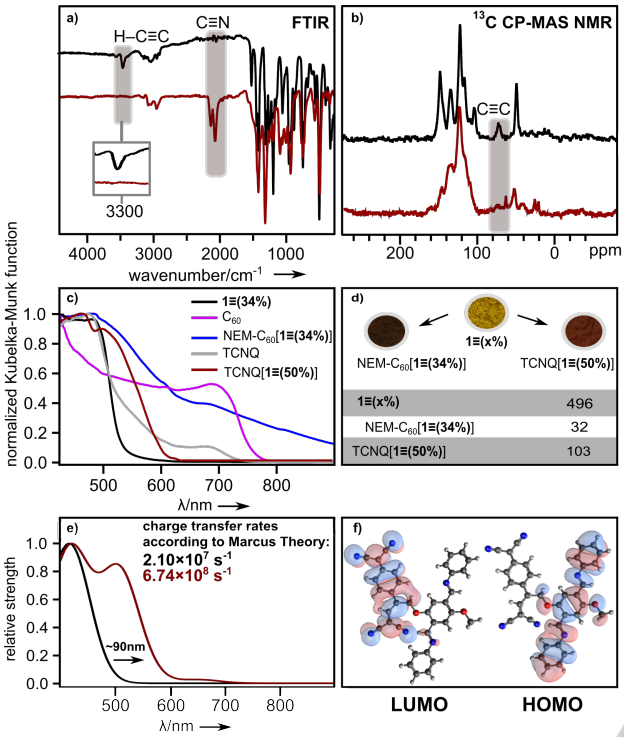

Figure 3. (a) FTIR spectra of **1≡(34%)** (black) and TCNQ[**1≡(50%)**] (red). Grey areas show the H–C≡C stretch present in **1≡(34%)** and absent in TCNQ[**1≡(50%)**] as well as appearance of the C≡N stretch in TCNQ[**1≡(50%)**]. (b) ^{13}C CP-MAS NMR spectra of **1≡(34%)** (black) and TCNQ[**1≡(50%)**] (red). (c) Normalized diffuse reflectance spectra of **1≡(34%)** (black), C_{60} (pink), NEM-C_{60}[**1≡(34%)**] (blue), TCNQ (grey), and TCNQ[**1≡(50%)**] (red). (d) Photographs of **1≡(x%)**, NEM-C_{60}[**1≡ (34%)**], and TCNQ[**1≡(50%)**]. The table shows the amplitude-weighted average lifetimes for **1≡(34%)**, NEM-C_{60}[**1≡ (34%)**], and TCNQ[**1≡(50%)**]. (e) The optical transition strength calculated for the COF-fragment (black) and TCNQ**[COF]**-fragment (red) and the corresponding electron transfer rates. The theory level is RPA TDDFT based on B3LYP-D3/6-31+G**. (f) Schematic representation of the frontier orbitals for the truncated molecular model comprised of the TCNQ**[COF]**-fragment.

resulting in further increases of conductivity in the range of two- to four-orders-of-magnitude with values of 5.06 × 10^{-8} S/cm, 1.08 × 10^{-5} S/cm, and 1.41 × 10^{-4} for COF, TCNQ[**1≡(50%)**], and TCNQ[**1≡(100%)**], respectively. The conductivity of NEM-C_{60}[**1≡(34%)**] increased to 3.63 × 10^{-5} S/cm when the material was doped with iodine. The detailed procedure of iodine doping can be found in the Supporting Information. The values obtained herein are among some of the highest values reported in COFs to date.[21–27] In addition, these conductivity studies are the first reports for COFs with covalently bound TCNQ moieties.

To shed light on how acceptor modulation and stacking (e.g., TCNQ moieties) could potentially affect COF properties, electronic structure calculations and electron transfer rates were estimated according to the Marcus theory[49] (Eq. 1).

$$k = 2\pi/\hbar \cdot |V_c|^2/\sqrt{(4\pi\lambda k_B T)} \cdot \exp\left(-\lambda/(4k_B T)\right) \quad (1)$$

where k = charge transfer rate, V_c = electron coupling, and λ = reorganization energy of the system; see the Supporting Information for more details. According to this model, TCNQ stacking inside of the COF could result in a *ca* 32-fold increase in electron transfer rates compared to the parent COF itself (see the Supporting Information for more details). In addition, the electronic structure analysis corroborates donor-acceptor alignment resulting in a bathochromic shift in optical transitions after TCNQ-integration (Figure 3) which is in good agreement with the experimental results (Figure 3).

In addition to "static" changes through acceptor incorporation inside the electron donating matrix, the electronic properties of COF materials could also be dynamically controlled through integration of photoresponsive molecules. To investigate this possibility, a spiropyran derivative, 1′,3′-dihydro-1′,3′,3′-trimethyl-6-nitrospiro[2*H*-1-benzopyran-2,2′-(2*H*)-indole] (SP, Figure S33), was encapsulated in **1≡(0%)**. In general, SP derivatives isomerize under UV irradiation to the charge-separated merocyanine form which could result in π-electron delocalization and possibly promote conductivity enhancement. Indeed, upon UV irradiation, a drastic color change from light yellow to dark brown was observed for SP@[**1≡(0%)**], indicating the transformation from the closed spiropyran form to the open merocyanine form (Figure S33).[50] Based on ^{1}H NMR spectroscopic analysis of the digested SP@**1≡(0%)**, one SP molecule was found per six –OMe units (Figure S32). Furthermore, after 30-min-UV irradiation, a 39%-increase in conductivity was observed in comparison with SP@**1≡(0%)** (5.38 × 10^{-11} S/cm). As a result, these studies could be considered as a blueprint for the development of stimuli-responsive crystalline doped COFs with dynamically controlled electronic behavior.

Due to the presence of redox-active building units, fullerene and TCNQ moieties, we studied the redox behavior of the prepared NEM-C_{60}[**1≡(34%)**] and TCNQ[**1≡(34%)**]. Significant modifications of the commonly used electrochemical setup were employed[51] since cyclic voltammetry studies of COFs are still relatively rare. The redox-active COFs (40 wt.%) were combined with carbon black (60 wt.%) and Nafion, and the obtained slurry was pipetted onto the tip of the electrode and dried under high vacuum. Cyclic voltammetry of TCNQ itself (1.0 × 10^{-4} M) was performed in a 0.1 M solution of tetrabutylammonium hexafluorophosphate in acetonitrile to afford one quasireversible reduction at E_p = –0.5 V and one oxidation at 0.1 V vs. saturated calomel electrode (SCE) (Figure S19). Comparison of the acquired CV data for TCNQ[**1≡(34%)**] to TCNQ itself, shows that both potentials of TCNQ[**1≡(34%)**] are less negative at E_p = –0.3 V and 0.2 V vs. SCE (Scheme 1), which could be evidence of the stronger electron accepting properties of the prepared material. Thus, inclusion of TCNQ in a COF matrix affects the redox potential, which enables this compound to be electrochemically sensed.[52] In comparison with C_{60} itself which exhibits four quasireversible reductions at E_p = –0.3 V, –0.7 V, –1.4 V, and –1.9 V in DMF vs. SCE, the NEM-C_{60} shows similar redox features at E_p = –0.9 V and –1.8 V (Figures S18 and S20). The reduction waves are more negative than that of pristine C_{60}, which is a known consequence of the saturation of a double bond on the C_{60} sphere.[53] The redox potentials of NEM-C_{60} (E_p = –0.9 V and –1.8 V) and NEM-C_{60}[**1≡(34%)**] (E_p = –1.2 V and –2.1 V vs. SCE) are also similar, with a slight shift in potential (Figures S20 and S21) supporting integration of NEM-C_{60} and reinforcement of the redox-active nature within the COF. Such electrochemical behavior (i.e., presence of two waves in the cyclic voltammogram) is comparable with C_{60}-based dimers in the literature,[53] with a reduced symmetry comparable to NEM-C_{60}. While CVs with integrated acceptors have been measured for other systems such as molecular rectangles,[52] these are the first studies, to the best

of our knowledge, that demonstrate redox-active behavior of TCNQ- and C_{60}-integrated COFs.

The aforementioned results demonstrate preparation of the first family members of purely organic, crystalline, porous scaffolds with covalently bound TCNQ and C_{60} moieties; integration of the latter ones not only resulted in increases in conductivity by eight-orders-of-magnitude, but affect the redox behavior of the material. Moreover, the interior of a COF was harnessed for the first time to perform a Sonogashira cross-coupling and [2+2] cycloaddition reactions, followed by ring opening of a strained intermediate in the case of the latter. The former reaction was probed for fluorophore tag integration that opens an avenue to control reaction progress inside of the COF. Notably, the reported purely organic covalently-integrated-acceptor scaffolds have the highest surface area and they are the first buckyball- and TCNQ-integrated COFs that exhibit redox behavior to date. Our theoretical analysis probing charge transfer rates within the Marcus theory as a function of TCNQ stacking within COFs showed a 32-fold increase in electron transfer rates compared to the parent COF itself. Despite the theory limitations, it is the first successful attempt to explain charge transfer in COFs using the Marcus theory that paves the way for further simulations of electronic structures and CT studies of hierarchical materials. Shifting from “static” tuning of the electronic structure, dynamic control of electronic properties in COFs as a function of external stimulus was achieved through spiropyran guest infiltration in the porous scaffold. Overall, this work demonstrates the potential for donor-acceptor alignment on the example of buckyball- and TCNQ-electron acceptors and COF-based donors for the development of porous and crystalline materials with tunable electronic structures that could open a new avenue for the rational design of electroactive and conductive multidimensional and multifunctional crystalline porous materials.

Experimental Section

Full experimental details can be found in the Supporting Information. CCDC 1883088 for 2-(4-(4,4-dicyano-2-(4-(dimethylamino)phenyl)butylidene)cyclohexa-2,5-dien-1-ylidene)malononitrile contains the supporting crystallographic data for this paper. These data can be obtained free of charge from The Cambridge Crystallographic Data Centre.

Acknowledgements

This work was supported by the NSF CAREER Award (DMR-1553634). N.B.S thanks the Cottrell Scholar Award from the Research Corporation for Science Advancement, Sloan Research Fellowship provided by Alfred P. Sloan Foundation, and Camille Dreyfus Teaching-Scholar Award provided by Henry and Camille Dreyfus Foundation. This material is based upon work partially supported by the National Science Foundation under Grant CHE-1565985, and in part by the National Science Foundation EPSCoR Program under NSF Award OIA-1655740. M.S. and B.W.L. acknowledge support of National Science Foundation under NSF Award DMR-1752615. This work made use of the South Carolina SAXS Collaborative. We also acknowledge USC's XPS user facility, as well as Dr. Stavros Karakalos for his help at the facility. Computations were performed on an HPC cluster funded by the National Science Foundation under Grant No. CHE-1048629.

Keywords: covalent-organic framework • donor acceptor interactions • electronic structure • fulleretic materials • redox-active

[1] M. Matsumoto, R. R. Dasari, W. Ji, C. H. Feriante, T. C. Parker, S. R. Marder, W. R. Dichtel, *J. Am. Chem. Soc.* **2017**, *139*, 4999–5002.
[2] C. R. DeBlase, W. R. Dichtel, *Macromolecules* **2016**, *49*, 5297–5305.
[3] A. J. Howarth, C. T. Buru, Y. Liu, A. M. Ploskonka, K. J. Hartlieb, M. McEntee, J. J. Mahle, J. H. Buchanan, E. M. Durke, S. S. Al-Juaid, J. F. Stoddart, J. B. DeCoste, J. T. Hupp, O. K. Farha, *Chem. Eur. J.* **2017**, *23*, 214–218.
[4] S. B. Alahakoon, C. M. Thompson, G. Occhialini, R. A. Smaldone, *ChemSusChem* **2017**, *10*, 2116–2129.
[5] S. Yang, W. Hu, X. Zhang, P. He, B. Pattengale, C. Liu, M. Cendejas, I. Hermans, X. Zhang, J. Zhang, J. Huang, *J. Am. Chem. Soc.* **2018**, *140*, 14614–14618.
[6] H. Wang, X. Dong, J. Lin, S. J. Teat, S. Jensen, J. Cure, E. V. Alexandrov, Q. Xia, K. Tan, Q. Wang, D. H. Olson, D. M. Proserpio, Y. J. Chabal, T. Thonhauer, J. Sun, Y. Han, J. Li, *Nat. Commun.* **2018**, *9*, 1745.
[7] Y. Wang, X. Zhao, H. Yang, X. Bu, Y. Wang, X. Jia, J. Li, P. Feng, *Angew. Chem. Int. Ed.* **2019**, *58*, 6316–6320.
[8] O. V. Boltalina, A. A. Popov, I. V. Kuvychko, N. B. Shustova, S. H. Strauss, *Chem. Rev.* **2015**, *115*, 1051−1105.
[9] S. A. Baudron, *CrystEngComm* **2016**, *18*, 4671–4680.
[10] A. Schneemann, V. Bon, I. Schwedler, I. Senkovska, S. Kaskel, R. A. Fischer, *Chem. Soc. Rev.* **2014**, *43*, 6062–6096.
[11] M. A. Petrukhina, *Dalton. Trans.,* **2019**, *48*, 5125–5130.
[12] J. Kurpiers, T. Ferron, S. Roland, M. Jakoby, T. Thiede, F. Jaiser, S. Albrecht, S. Janietz, B. A. Collins, I. A. Howard, D. Neher, *Nat. Commun.* **2018**, *9*, 2038.
[13] M. Adams, N. Baroni, M. Oldenburg, F. Kraffert, J. Behrends, R. W. MacQueen, R. Haldar, D. Busko, A. Turshatov, G. Emandi, M. O. Senge, C. Wöll, K. Lips, B. S. Richards, I. A. Howard, *Phys. Chem. Chem. Phys.*, **2018**, *20*, 29142–29151.
[14] D. E. Williams, E. A. Dolgopolova, D. C. Godfrey, E. D. Ermolaeva, P. J. Pellechia, A. B. Greytak, M. D. Smith, S. M. Avdoshenko, A. A. Popov, N. B. Shustova, *Angew. Chem. Int. Ed.* **2016**, *55*, 9070–9074.
[15] J. Sukegawa, C. Schubert, X. Zhu, H. Tsuji, D. M. Guldi, E. Nakamura, *Nat. Chem.* **2014**, *6*, 899–905.
[16] C.-Z. Li, H.-L. Yip, A. K.-Y. Jen, *J. Mater. Chem.* **2012**, *22*, 4161–4177.
[17] C. D. Wessendorf, R. Eigler, S. Eigler, J. Hanisch, A. Hirsch, E. Ahlswede, *Sol. Energy Mater. Sol. Cells* **2015**, *132*, 450–454.
[18] A. Hirsch, *The Chemistry of Fullerenes*, John Wiley And Sons, Inc., **2008**.
[19] D. M. Guldi, *Chem. Commun.* **2000**, 321–327.
[20] D. Josa, J. Rodríguez-Otero, E. M. Cabaleiro-Lago, L. A. Santos, T. C. Ramalho, *J. Phys. Chem. A* **2014**, *118*, 9521−9528.
[21] H. Yang, S. Zhang, L. Han, Z. Zhang, Z. Xue, J. Gao, Y. Li, C. Huang, Y. Yi, H. Liu, Y. Li, *ACS Appl. Mater. Interfaces* **2016**, *8*, 5366–5375.
[22] H. S. Sasmal, H. B. Aiyappa, S. N. Bhange, S. Karak, A. Halder, S. Kurungot, R. Banerjee, *Angew. Chem. Int. Ed.* **2018**, *57*, 10894–10898.
[23] S.-L. Cai, Y.-B. Zhang, A. B. Pun, B. He, J. Yang, F. M. Toma, I. D. Sharp, O. M. Yaghi, J. Fan, S.-R. Zheng, W.-G. Zhang, Y. Liu, *Chem. Sci.,* **2014**, *5*, 4693–4700.
[24] S. Duhović, M. Dincă, *Chem. Mater.* **2015**, *27*, 5487–5490.
[25] H. Guo, J. Wang, Q. Fang, Y. Zhao, S. Gu, J. Zheng, Y. Yan, *CrystEngComm*, **2017**, *19*, 4905–4910.
[26] D. A. Vazquez-Molina, G. S. Mohammad-Pour, C. Lee, M. W. Logan, X. Duan, J. K. Harper, F. J. Uribe-Romo, *J. Am. Chem. Soc.* **2016**, *138*, 9767–9770.
[27] E. Jin, M. Asada, Q. Xu, S. Dalapati, M. A. Addicoat, M. A. Brady, H. Xu, T. Nakamura, T. Heine, Q. Chen, D. Jiang, *Science* **2017**, *357*, 673–676.
[28] X. Feng, X. Ding, D. Jiang, *Chem. Soc. Rev.*, **2012**, *41*, 6010–6022.
[29] M. S. Lohse, T. Bein, *Adv. Funct. Mater.* **2018**, *28*, 1705553.
[30] R. P. Bisbey, W. R. Dichtel, *ACS Cent. Sci.* **2017**, *3*, 533–543.

[31] A. M. Rice, E. A. Dolgopolova, B. J. Yarbrough, G. A. Leith, C. R. Martin, K. S. Stephenson, R. A. Heugh, A. J. Brandt, D. A. Chen, S. G. Karakalos, M. D. Smith, K. B. Hatzell, P. J. Pellechia, S. Garashchuk, N. B. Shustova, *Angew. Chem. Int. Ed.* **2018**, *57*, 11310–11315.

[32] S. Goswami, D. Ray, K.-I. Otake, C.-W. Kung, S. J. Garibay, T. Islamoglu, A. Atilgan, Y. Cui, C. J. Cramer, O. K. Farha, J. T. Hupp, *Chem. Sci.*, **2018**, *9*, 4477–4482.

[33] A. A. Talin, A. Centrone, A. C. Ford, M. E. Foster, V. Stavila, P. Haney, R. A. Kinney, V. Szalai, F. El Gabaly, H. P. Yoon, F. Léonard, M. D. Allendorf, *Science.* **2014**, *343*, 66–69.

[34] S. B. Kalidindi, C. Wiktor, A. Ramakrishnan, J. Weßing, A. Schneemann, G. Van Tendeloo, R. A. Fischer, *Chem. Commun.*, **2013**, *49*, 463–465.

[35] J. Zhang, L. Wang, N. Li, J. Liu, W. Zhang, Z. Zhang, N. Zhou, X. Zhu, *CrystEngComm*, **2014**, *16*, 6547–6551.

[36] S. Zhao, B. Dong, R. Ge, C. Wang, X. Song, W. Ma, Y. Wang, C. Hao, X. Guo, Y. Gao, *RSC Adv.*, **2016**, *6*, 38774–38781.

[37] H. Xu, J. Gao, D. Jiang, *Nat. Chem.* **2015**, *7*, 905–912.

[38] A. M. Rice, E. A. Dolgopolova, N. B. Shustova, *Chem. Mater.* **2017**, *29*, 7054–7061.

[39] L. Chen, K. Furukawa, J. Gao, A. Nagai, T. Nakamura, Y. Dong, D. Jiang, *J. Am. Chem. Soc.* **2014**, *136*, 9806–9809.

[40] D. D. Medina, V. Werner, F. Auras, R. Tautz, M. Dogru, J. Schuster, S. Linke, M. Döblinger, J. Feldmann, P. Knochel, T. Bein, *ACS Nano* **2014**, *8*, 4042–4052.

[41] M. Dogru, M. Handloser, F. Auras, T. Kunz, D. Medina, A. Hartschuh, P. Knochel, T. Bein, *Angew. Chem. Int. Ed.* **2013**, *52*, 2920–2924.

[42] J. Guo, Y. Xu, S. Jin, L. Chen, T. Kaji, Y. Honsho, M. A. Addicoat, J. Kim, A. Saeki, H. Ihee, S. Seki, S. Irle, M. Hiramoto, J. Gao, D. Jiang, *Nat. Commun.* **2013**, *4*, 2736.

[43] P. Hu, K. Du, F. Wei, H. Jiang, C. Kloc, *Cryst. Growth Des.* **2016**, *16*, 3019–3027.

[44] K. Kanai, K. Akaike, K. Koyasu, K. Sakai, T. Nishi, Y. Kamizuru, T. Nishi, Y. Ouchi, K. Seki, *Appl. Phys. A* **2009**, *95*, 309–313.

[45] H. Alves, R. M. Pinto, E. S. Maçôas, *Nat. Commun.* **2013**, *4*, 1842.

[46] F. D'Souza, O. Ito, *Coord. Chem. Rev.*, **2005**, *249*, 1410–1422.

[47] M. Usman, S. Mendiratta, S. Batjargal, G. Haider, M. Hayashi, N. Rao Gade, J.-W. Chen, Y.-F. Chen, K.-L. Lu, *ACS Appl. Mater. Interfaces* **2015**, *7*, 22767–22774.

[48] R. López, R. Gómez, *J. Sol-Gel Sci. Technol.* **2012**, *61*, 1–7.

[49] R. A. Marcus, *Rev. Mod. Phys.* **1993**, *65*, 599–610.

[50] A. M. Rice, C. R. Martin, V. A. Galitskiy, A. A. Berseneva, G. A. Leith, N. B. Shustova, *Chem. Rev.* **2019**, DOI: 10.1021/acs.chemrev.9b00350.

[51] C. R. DeBlase, K. E. Silberstein, T.-T. Truong, H. D. Abruña, W. R. Dichtel, *J. Am. Chem. Soc.* **2013**, *135*, 16821–16824.

[52] T. Rajendran, B. Manimaran, R.-T. Liao, Y.-H. Liu, P. Thanasekaran, R.-J. Lin, I.-J. Chang, P.-T. Chou, R. Ramaraj, S. Rajagopal, K.-L. Lu, *Dalton. Trans.*, **2010**, *39*, 2928–2935.

[53] A. Sastre-Santos, C. Parejo, L. Martin-Gomis, K. Ohkubo, F. Fernández-Lázaro, S. Fukuzumi, *J. Mater. Chem.*, **2011**, *21*, 1509–1515.

10.1002/anie.201914233

WILEY-VCH

COMMUNICATION

Sometimes a journey into the deep confines of the forest can lead to new discoveries. Electron acceptors prepared themselves for travel into the unknown of the COF electron-donating “forest”. Instead of getting lost in the deep, dark forest, the acceptor-based (purely organic) covalently bound, crystalline and porous scaffolds exhibited not only increases in conductivity, but also retention of the redox-active nature.

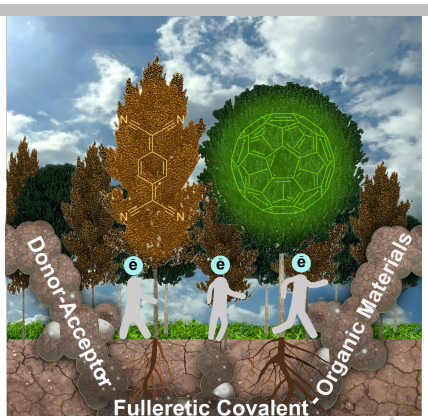

Gabrielle A. Leith,[§] Allison M. Rice,[§] Brandon J. Yarbrough,[§] Anna A. Berseneva, Richard T. Ly, Charles N. Buck III, Denis Chusov, Amy J. Brandt, Donna A. Chen, Benjamin W. Lamm, Morgan Stefik, Kenneth S. Stephenson, Aaron K. Vannucci, Perry J. Pellechia, Sophya Garashchuk, and Natalia B. Shustova Page No. – Page No.*

A Dual Threat: Redox-Activity and Electronic Structures of Well-Defined Donor-Acceptor Fulleretic Covalent-Organic Materials